Research Article | Vol. 30, No. 1 / 3 Jan 2022 / Optics Express 576

Optics EXPRESS

Bandwidth optimization for the Advanced Volume Holographic Filter

PEDRO ENRIQUE ALCARAZ, GREGORY NERO, AND PIERRE-ALEXANDRE BLANCHE*

Wyant College of Optical Sciences, University of Arizona, 1630 E University Blvd., Tucson, AZ 85721, USA
**pablanche@optics.arizona.edu*

Abstract: The high angular and spectral selectivity of volume holograms have been used in fields like astronomy, spectroscopy, microscopy, and optical communications to perform spatial filtering and wavefront selection. In particular, imaging systems that utilize volume holograms to perform range-based wavefront selection have allowed for the potential to have full 24-hour observational custody of artificial satellites by enabling daytime observations. We previously introduced the Advanced Volume Holographic Filter (AVHF) which demonstrated a significant system bandwidth improvement while maintaining high angular selectivity. Presented here is a theoretical basis for maximizing the bandwidth of the AVHF systems. We experimentally demonstrate an improvement of 40.7-41.4x compared to the un-optimized AVHF systems.

1. Introduction

Volume holograms can be used in optical imaging systems to play the role of a spatial filter and to select particular wavefront shapes [1]. The high spectral and angular selectivity of volume holograms have been employed for use in spatio-spectral imaging [2–4], confocal microscopy [5–7], and have enabled advances in wavelength division/spatial mode multiplexing [8,9]. These thick holographic elements have also been incorporated into imaging systems designed to discriminate and select wavefronts based on distance [10–14,16].

Of particular relevance is the use of volume holographic filters to perform ground-based detection and ranging of satellites [15]. The work most recently done by Chen et al. [14] and others [10,16] focuses on daytime observation of satellites, which is a unique challenge because of the noise introduced by daytime Rayleigh-scattered light from the atmosphere. These systems utilized a volume hologram as a spatio-spectral filter for the improvement of imaging SNR via wavefront selection. The inherent thickness of the holographic elements required for wavefront selection necessitates a narrow spatial and spectral bandwidth imposed via the Bragg condition. Unfortunately, using a single thick volume holographic element to filter the wavefront also dramatically reduces the wavelength bandwidth. In the case of a polychromatic sources the volume hologram effectively reduces the throughput of the instrument which negatively affects the imaging system's SNR for wavelengths outside the Bragg wavelength.

In this paper, we expand upon our previous work where we developed the Advanced Volume Holographic Filter (AVHF) [17]. The AVHF demonstrated an improvement to the SNR of systems where polychromatic signal and noise are located at different distances within the same line of sight using a combination of two holographic elements. Herein our goal is to build a general framework to derive, simulate, and experimentally demonstrate a way to maximize the full-width-half-max spectral bandwidth of the AVHF system to meet the design constraints of general systems requiring substantial spatial selectivity, per wavefront selection, and spectral bandwidths larger than those imposed by the Bragg condition.

#444101 https://doi.org/10.1364/OE.444101
Journal © 2022 Received 7 Oct 2021; revised 24 Nov 2021; accepted 7 Dec 2021; published 23 Dec 2021

Optics EXPRESS

2. Theoretical background

The Advanced Volume Holographic Filter (AVHF) is a holographic system capable of broadband depth-based wavefront selection. The system is composed of two holographic elements: a pre-dispersor (PD) and a volume holographic filter (VHF). The performance of the system can best be characterized by the angular and wavelength selectivity. As previously demonstrated in other works, VHF's have a very high angular and spectral selectivity allowing for narrow-band depth based wavefront selection [13,14,16]. In prior work we have demonstrated that a PD element that is sufficiently thin can be used to modify the propagation vectors of individual wavelengths whilst maintaining a high diffraction efficiency across a large spectral bandwidth. Thus, a PD can be used as Bragg matching element; where the PD diffracted spectra can be coupled onto a VHF for depth-based selection.

The diffractive behavior of a volume hologram can best be characterized via the Klein and Cook criteria; where holograms with a Q parameter less than 1 operate in the Raman-Nath regime and holograms with a Q parameter greater than 10 operate in the Bragg regime [18]. The Q parameter can be calculated via Eq. (1),

$$Q = \frac{2\pi\lambda_R L}{n_0 \Lambda^2 \cos\theta} \tag{1}$$

where, λ_R refers to the volume hologram recording wavelength, n_0 to the material's index, Λ to the spatial period between gratings, L to the length/thickness of the recorded hologram, and θ to the angle of incidence.

The holographic elements used in the AVHF system are considered thick holograms, with Q > 10. The theoretical Q for the PD's we plan to implement has a Q ~ 250 while the volume holographic filter has a Q ~ 30,000. Herein we will make explicit reference to effective thickness, denoted as L_{eff}, to refer to the optical thickness of the diffraction grating, i.e. the thickness of the observed Bragg response of the material. References made to thickness, L, will only pertain to the material's physical thickness. This treatment has has been widely used in literature to highlight that oftentimes the recorded volume thickness $L_{\text{eff}} < L$ and in rare cases $L_{\text{eff}} = L$ [19,20].

2.1. Volume hologram diffraction

The diffractive behavior of a thick transmission volume hologram can best be characterized via the grating equation:

$$\Lambda \sin\theta_i + \Lambda \sin\theta_d = \frac{m\lambda}{n}; \quad m \in \mathbb{Z} \tag{2}$$

where rearranging Eq. (2) for a fixed volume grating, the following relationship between diffraction angle and angle of incidence is expected:

$$\theta_d(\lambda) = \arcsin\left(\frac{\lambda}{\Lambda} - \sin\theta_i\right) \tag{3}$$

Here, Λ refers to the grating period, $\Lambda = \frac{2\pi}{|\mathbf{K}|}$, θ_i the angle of incidence with respect to the plane normal to the grating vector, θ_d the angle of diffraction with respect to the plane normal to the grating vector, m is the diffraction order (m=1 in the case of thick holograms operating in the Bragg regime), n is the medium's index, and λ is the wavelength of the incident wavefront/ray. The diffractive behavior of a thick holographic element is summarized in Fig. (1) where both incident monochromatic and polychromatic diffraction schemes are shown. Volume holograms that are sufficiently thick typically display stringent Bragg selection criteria, i.e. the diffraction of an incident wavefront is highly dependent on the angle of incidence, θ_i. Maximal diffraction efficiency occurs at the Bragg angle, where $\theta_i = \theta_B$, Δn refers to the material index modulation, L

Optics EXPRESS

the recorded length, and λ the wavelength of the incident wavefront.

$$\eta_B = \sin^2\left(\frac{\pi \Delta n L}{\lambda \cos\theta_B}\right) \tag{4}$$

The diffraction efficiency for an incident monochromatic wavefront can be calculated using Kogelnik's coupled wave equations, Eq. (5–6) [23].

$$\eta(\theta_i) = \frac{\sin^2(\sqrt{\Delta\theta_i}\frac{\pi \Delta n L}{\lambda \cos\theta_i})}{\Delta\theta_i} \tag{5}$$

$$\Delta\theta_i = 1 + \left(\frac{2n \sin\theta_B(\sin\theta_i - \sin\theta_B)}{\Delta n}\right)^2 \tag{6}$$

Moreover, ZEMAX's OpticStudio can also simulate the diffraction efficiency of an optical system, composed of either a single or multiple holographic elements, via ray-trace. In this study, we will implement OpticStudio's Diffraction Efficiency scheme to model out holographic elements and systems.

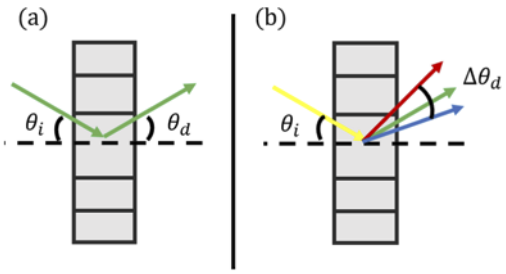

Fig. 1. Schematic demonstrating wavelength dependent diffraction through a thick- volume holographic element; where (a) the incident wavefront is collimated and monochromatic (b) the incident wavefront is collimated and polychromatic.

2.2. *Volume hologram coupling*

As previously demonstrated, dispersive elements can be coupled to volume holographic filters to increase the diffracted spectral bandwidth whilst maintaining angular selectivity of a system [17]. Described is the analytical basis for PD-VHF coupling; where optimal recording parameters required to Bragg match a predisperser onto a volume holographic filter are prescribed.

The Bragg angle of a fixed holographic grating can be determined for an arbitrary wavelength using the following equations; where Eq. (7) provides the relationship between the grating period Λ and the recording conditions θ_R, λ_R, Eq. (8) provides the relationship between the Bragg angle of the recording wavelength λ_R and the grating vector Λ, and Eq. (9) combines Eq. (7–8) to derive the relationship between the wavelength dependent Bragg angle $\theta_B(\lambda)$ and an arbitrary incident wavelength λ:

$$\Lambda = \frac{\lambda_R}{2\sin\theta_R} \tag{7}$$

$$\sin\theta_B = m\frac{\lambda_R}{2\Lambda}; m \in \mathbb{N} \tag{8}$$

$$\theta_B(\lambda) = \arcsin\left(\frac{\lambda}{\lambda_R}\sin\theta_R\right) \tag{9}$$

In order to efficiently couple two holographic elements the diffracted rays from the first hologram must match the Bragg condition of the second holographic element, $\theta_d(\lambda) = \theta_B(\lambda)$.

Optics EXPRESS

Due to the inherent dispersion asymmetry between red, $\lambda_{(+)}$, and blue, $\lambda_{(-)}$, wavelengths, relative to the recording wavelength, optimization of the diffracted spectra for a particular AVHF system is dependent on i) the VHF recording angle, i.e. working angular selectivity, and the predisperser diffraction angle and spectral bandwidth, see Fig. (2). To generate sets of working solutions we solve for Eq. (10).

$$\Delta\theta_d(\lambda) = \Delta\theta_B(\lambda) \tag{10}$$

$$\Delta\theta_d(\lambda) = \arcsin\left(\frac{-2\lambda_{(+)}}{\lambda_{\mathrm{R}}}\sin\theta_{\mathrm{R,PD}} + \sin\theta_{\mathrm{R,PD}}\right) - \arcsin\left(\frac{-2\lambda_{(-)}}{\lambda_{\mathrm{R}}}\sin\theta_{\mathrm{R,PD}} + \sin\theta_{\mathrm{R,PD}}\right) \tag{11}$$

$$\Delta\theta_B(\lambda) = \arcsin\left(\frac{\lambda_{(+)}}{\lambda_R}\sin\theta_{\mathrm{R,VHF}}\right) - \arcsin\left(\frac{\lambda_{(-)}}{\lambda_R}\sin\theta_{\mathrm{R,VHF}}\right) \tag{12}$$

Note that Eq. (10) is dependent on the range $\Delta\lambda = \lambda_{(+)} - \lambda_{(-)}$. To find the PD recording angle, $\theta_{\mathrm{R,PD}}$, that will Bragg match an incident wavefront onto a VHF, we moved to fix the VHF recording conditions, λ_R, as well as the VHF recording angle, $\theta_{\mathrm{R,VHF}}$, to generate a solution for $\theta_{\mathrm{R,PD}}$ as a function of $\theta_{\mathrm{R,VHF}}$:

$$\theta_{\mathrm{R,PD}}(\theta_{\mathrm{R,VHF}}) = \arcsin\left(\frac{\sqrt{\alpha\sqrt{\beta}}}{\gamma}\right) \tag{13}$$

Refer to the Supplement 1 for values pertaining to $\alpha, \beta,$ and γ. As mentioned previously, the PD recording parameters are not only dependent on the VHF parameters but also on the Bragg matching wavelengths of interest: $\Delta\lambda = \lambda_{(+)} - \lambda_{(-)}$. Therefore, for any given range $\Delta\lambda$ there exist multiple solutions that can Bragg match the PD diffracted spectrum onto the VHF element with varying system spectral bandwidths. Within the solution subspace, see Fig. (3), we are interested in finding a solution with a maximal diffracted spectral bandwidth (FWHM).

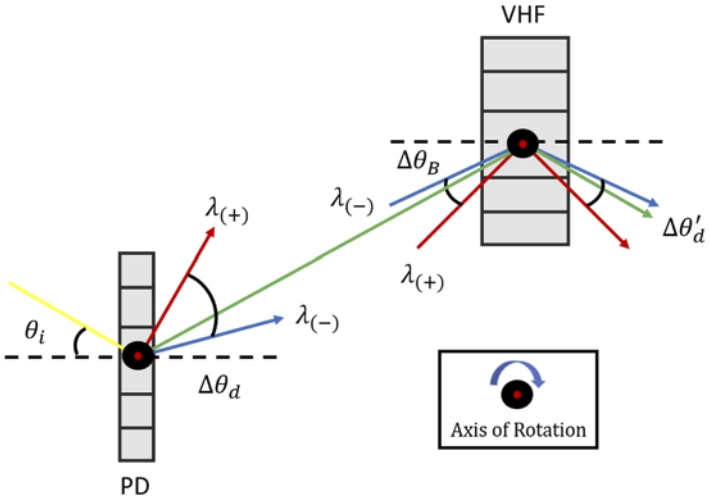

Fig. 2. Schematic demonstrating wavelength dependent diffraction $\Delta\theta_d$ and the required Bragg incidence $\Delta\theta_B$ for diffraction through a coupled thick- volume hologram system; where the incident wavefront is collimated and polychromatic.

Optics EXPRESS

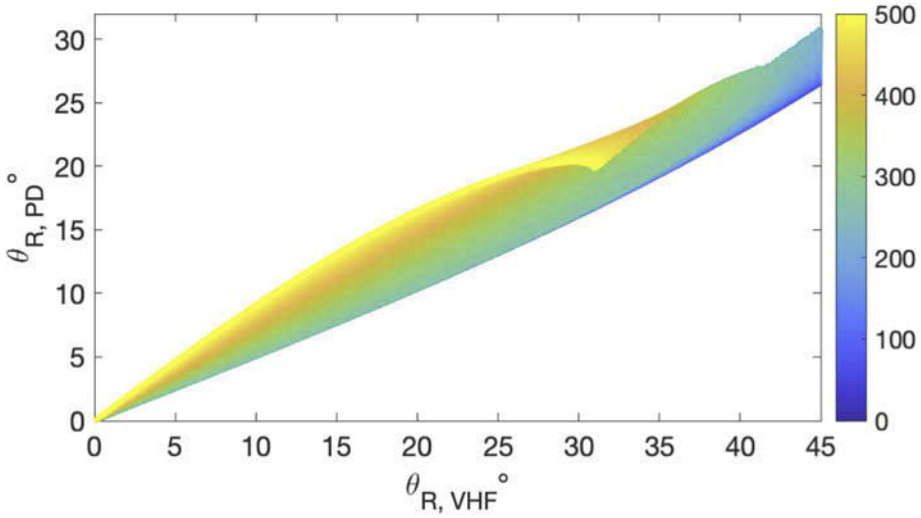

Fig. 3. Schematic presents the PD recording angle(s) $\theta_{R,PD}$ solution subspace necessary to Bragg match in incident polychromatic wave-front onto a VHF with recording angle $\theta_{R,PD}$ recorded at $\lambda = 532$ nm. The with solution subspace presented probes $\Delta\lambda$ ranging from $\Delta\lambda = 1$ to $\Delta\lambda = 500$ as denoted by the color bar.

3. Materials and methods

We demonstrate spectral broadening using the coupled AVHF system under laboratory conditions and compare results to simulation. In this process two AVHF systems were assessed: System I with a VHF operating at 45° and System II with a VHF operating at 22.5°.

3.1. AVHF spectral bandwidth optimization

The solution set of interest in this study is the PD recording angle that produces the broadest spectral bandwidth (FWHM). In order to find the solution set we modeled a number of AVHF systems in ZEMAX's OpticStudio 21.1. There was only one degree of freedom the the modeled systems; namely, the PD recording angle $\theta_{\mathrm{R,PD}}$ which is dependent on Eq. (11) and $\Delta\lambda$. Otherwise the VHF recording angle, $\theta_{\mathrm{R,VHF}}$, constrained all other free variables in the AVHF system; where, PD and VHF $\hat{x}$ tilt relative to the optical axis $\hat{z}$ are dependent on the VHF recording angle. The VHF rotation is given by $\theta_{\hat{x},\mathrm{VHF}} = |\theta_{\mathrm{R,VHF}}| - |\theta_{\mathrm{R,PD}}|$ and the PD rotation is given by $\theta_{\hat{x},\mathrm{PD}} = |\theta_{\mathrm{R,PD}}|$, see Fig. (2). The system is oriented such that $\lambda = 532nm$ is always incident on the VHF element at an angle of $\theta_i = \theta_{\mathrm{R,VHF}}$.

The angular and spectral diffraction efficiencies were calculated via ray-trace; where ZEMAX's OpticStudio Version 21.1 can solve Kogelnik's coupled wave equations to produce efficiency measurements, see Eq. (5–6). The light source was unpolarized, located at -infinity, with a system aperture 10mm away from the PD element. The separation between the PD and VHF elements was fixed to 10 mm, the separation between the VHF element and the imaging plane also remained fixed at 10 mm, see Fig. (4).

3.2. Predisperser recording angle

In this study we are looking for a solution to maximize the FWHM diffracted spectral bandwidth of an arbitrary VHF element. Through simulation we derived a relation between PD recording angle and VHF recording angle. This relation can be used to approximate the PD recording angle

Optics EXPRESS

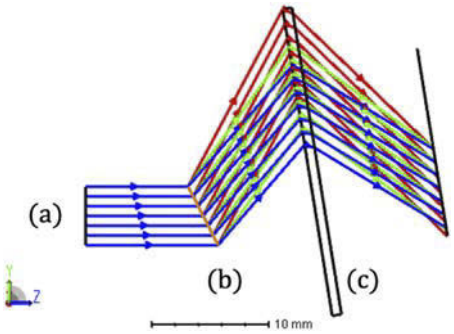

Fig. 4. Ray-trace denoting the AVHF arrangement in ZEMAX's OpticStudio 21.1 (a) a collimated polychromatic wavefront is incident onto a predispersive element (b) who's m = 1 diffraction mode is incident onto a VHF element (c) who's m = 1 diffracted mode is assessed for angular and spectral selectivity. The $\hat{y}$ and $\hat{z}$ axes are provided, with the $\hat{x}$ perpendicular to the yz plane.

that will Bragg match the largest spectral bandwidth of an incoming wavefront to a VHF:

$$\theta_{R,PD} = 0.00450(\theta_{R,VHF})^2 + 0.363(\theta_{R,VHF}) + 1.265^\circ \tag{14}$$

see Supplementary Section for derivation. Summarized below are two examples of PD/VHF coupling: System I featuring a VHF operating at 45° and System II featuring a VHF operating at 22.5°. Using Eq. (14), one can derive the PD recording angle to maximize spectral coupling: $\theta_{PD} = 26.71^\circ$ and $\theta_{PD} = 11.71^\circ$ for AVHF systems operating at 45° and 22.5° respectively. The simulated diffracted spectra as a function of bandwidth parameter $\Delta\lambda$ for the AVHF systems are provided in Fig. (5), where the diffraction efficiency of the individual AVHF elements, PD and VHF, were optimized via the effective hologram length. In this case, AVHF System I consisted of a VHF element with $L_{VHF} = 1.4mm$ and PD $L_{PD} = 14\mu m$ generating a PD working at 90% diffraction efficiency and a VHF at 73%. AVHF System II consisted of a VHF element with $L_{VHF} = 1.4mm$ and PD $L_{PD} = 11\mu m$ generating a PD working at 92% diffraction efficiency and a VHF at 90%.

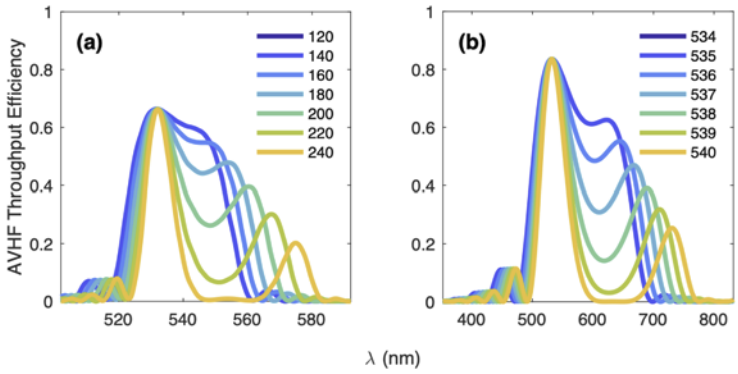

Fig. 5. Simulated AVHF throughput efficiency curves for AVHF System I (a) and System II (b) featuring VHF recorded at 45 and 22.5 respectively. The individual curves on each subplot represent the efficiency curves associated with a specific $\Delta\lambda$ (nm) and by association, a specific PD recording angle, the $\Delta\lambda$ (nm) probed in (a) range from [120,240], while the the $\Delta\lambda$ probed in (b) range from [534,540].

Optics EXPRESS

Figure (5) demonstrates the simulated spectral diffraction efficiency as a function of $\Delta\lambda$. As mentioned previously, there exists a solution subspace, see Fig. (3), form which we hope to find the optimal PD recording parameters. By varying $\Delta\lambda$ we can find the broadest AVHF diffracted spectral bandwidth and identify the optimal PD recording angle, see Eq. (10–12). As shown the curves increase (from purple to yellow) in steps between the following rages, in nanometers, which will be given as: [$\Delta\lambda_{min}$, $\Delta\lambda_{max}$, step size]: (a) [120, 240, 20], (b) [534, 540, 1]. Among these curves in each subplot there will be one solution that yields the highest integrated efficiency. The curve with the highest integrated efficiency for each VHF recording angle corresponds to the "probed solutions" that we present in Figures S2-S3, used to generate Eq. (14).

3.3. Hologram recording arrangement

All holograms were recorded using an Nd:YAG laser with center wavelength at λ_R = 532 nm. Both the signal and reference arms were collimated and incident to the holographic recording material in a symmetric configuration, i.e. the signal beam is incident on the VH at $-\theta_R$ and the reference, beam is incident on the VH at θ_R.

3.4. Materials for volume hologram

The material used to record the PD elements was the Bayfol HX200 photopolymer with thicknesses of 16μm. The exposure energy required for the Bayfol HX thin-volume holograms were 25 mJ/cm^2, after that the samples were exposed to an incoherent halogen white light source for ~5 min to fix the recorded index modulation.

The material used to record the VHF elements was phenanthrenequinone- doped poly-(methyl-methacrylate), (PQ-doped PMMA), allowing for VH thicknesses > 1mm. The exposure energy required for the thick-volume holograms where 1,800 J/cm^2. Studies have found that grating strength can be increased by allowing unexposed PQ molecules to diffuse into exposed regions, generating a homogeneous post-exposure PQ concentration across the sample; therefore as a post exposure treatment, the PQ-doped PMMA holograms were placed in a dark container for 24hrs, allowing for unexposed PQ diffusion [21,22]. Thereafter, the hologram was exposed to an incoherent halogen white light source for 24hrs, see Supplement 1 for PQ-PMMA synthesis procedure.

3.5. Holograms characterization

The measurements of angular selectivity and diffraction efficiency were carried out by illuminating the PD and VHF to a collimated beam from an Nd:YAG laser with center wavelength at λ = 532nm. The holograms were mounted on a manual rotation stage; measurements were taken at $\theta_B \pm \Delta\theta$. The zero and first order diffracted beam intensities were used to characterize the angular selectivity and effective thickness of the holograms. The measurements of spectral selectivity were carried out by illuminating the PD and VHF to a collimated beam from a NKT SuperK COMPACT supercontinuum laser. The holograms were mounted on a manual rotation stage; spectral measurements were taken at the zero and first order diffracted beams using an OceanOptics USB4000 fiber spectrometer.

Since the first-order diffraction is spectrally disperse an integration sphere was utilized to record the diffracted spectrum. This procedure was used to avoid wavelength dependent coupling losses and allowed for repeatable measurements.

The angular and spectral selectivity of the individual AVHF elements and the AVHF system were compared to simulated holographic elements in ZEMAX's OpticStudio 21.1. The effective thicknesses and recording parameters of the holographic elements in the AVHF system were used to generate the simulated angular and spectral selectivity's of each element as well as the those of the entire system.

Optics EXPRESS

4. Results and discussion

Two AVHF systems where characterized. System I is comprised of a 26.7° PD element coupled to a 45° VHF. System II is comprised of a 11.7° PD element coupled to a 22.5° VHF. The goal is to create systems with stringent spatial selectivity for wavefront selection via a thick volume hologram and increase the spectral bandwidth (FWHM) of the system by coupling a predispersive element. The PD element recording angles were derived via Eq. (14) with efforts aimed at optimizing the diffracted spectral bandwidth of the AVHF systems, refer to Fig. (5) and Supplement 1.

4.1. Characterization of materials

The angular and spectral selectivity measurements for the individual AVHF elements were fitted to expected values via ZEMAX'S OpticStudio 21.1. The angular and spectral selectivity measurements were used to derive general parameters such as the effective hologram thickness and index modulation Δn, see Fig. (6) for fitted models and Table 1 for the retrieved holographic element effective thickness, index modulation, and material index.

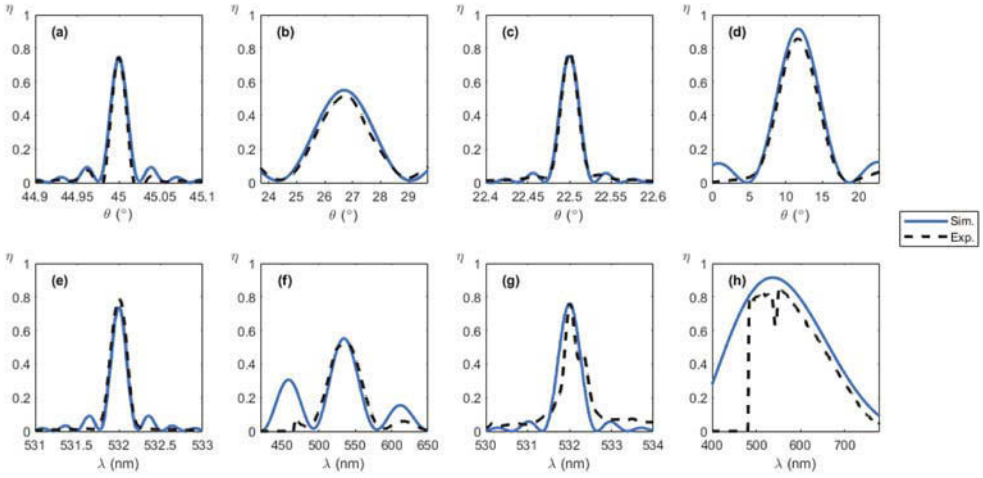

Fig. 6. (a-d) Angular selectivity measurements of AVHF System I (a-b) and AVHF System II (c-d); where (a) and (c) are measurements obtained from the VHF element and (b) and (d) are measurements obtained from the predispersive element. Similarly, (e-h) present spectral selectivity measurements of AVHF System I (e-f) and AVHF System II (g-h); where (e) and (g) are measurements obtained from the VHF element and (f) and (h) are measurements obtained from the predispersive element.

Table 1. Denotes the recovered volume hologram material properties. Each parameter was recovered by fitting the angular and spectral selectivity of the optical element to simulation (Kogelnik).

System	Element	L_{eff} (mm)	Δn	n
AVHF-SI	45° VHF	1.400	2.00E-04	1.505
	26.7° PD	0.011	2.50E-02	1.493
AVHF-SII	22.5° VHF	2.000	1.00E-04	1.505
	11.7° PD	0.014	2.00E-02	1.493

Optics EXPRESS

Figure (6) presents the angular and spectral selectivity curves from the empirical data (black) and the modeled data (blue). Based on prior work and material characterization we determined that the material index for 16 μm Bayfol is ~1.505, with an index modulation, Δn ~0.03, with a typical effective thickness $L_{eff}<16\mu m$. As for PQ-doped PMMA, the samples synthesized were 3 mm in thickness; thus, we expect an effective recorded thickness $L_{eff}<3mm$. The reported material index modulations for PQ-PMMA vary in literature, ranging from $1.00E-04<\Delta n<$ 3.00E-04, with an expected material index of n = 1.493 [24,25]. The angular and spectral diffraction efficiency curves allowed us to approximate the material characteristics for each holographic element. The recovered material properties are summarized in Table 1 and are well within the expected/previously reported material parameters.

4.2. PD to VHF Bragg matching efficiency

Here we present the AVHF system (I & II) spectral bandwidth optimization results and compare them to the OpticStudio simulated models. Figure (7) presents the spectra of light incident on the AVHF system, referred to as white light (WL), and the diffracted spectral curves, normalized and dependent on WL, for both empirical and simulated (s) models. Note that WL spectral bandwidth limits the diffraction of the PD elements, where there is no light $\lambda<460nm$ incident on the system. When calculating the spectral diffraction efficiency data $\lambda \leq 460nm$ was removed as it quickly diverges to infinity, however, efforts where made to retrieve data up to the 460nm cutoff.

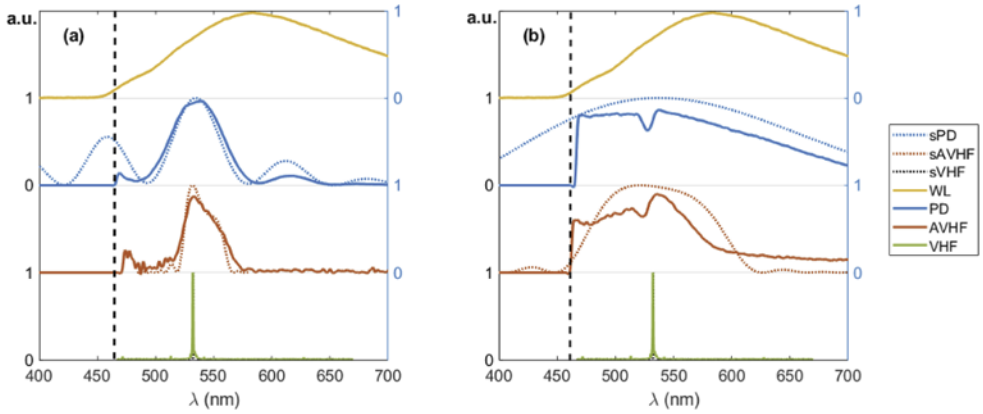

Fig. 7. Spectral data collected from (a) AVHF System I and (b) AVHF System II. The yellow curve represents the white light spectra incident on the system. Diffracted spectra from the PD and the overall AVHF system presented by the blue and orange curves respectively. The green curve represents the diffracted spectra from the uncoupled thick volume hologram used in the AVHF system. The dashed curves (blue, orange, and green) are OpticStudio simulated diffraction spectra recovered via element characterization, labeled s- for simulated.

From the data presented in Fig. (7) we can clearly observe a substantial increase in the diffracted spectral bandwidth due the AVHF system (orange), in both (a) and (b); where, (a) features a 26.7° PD element coupled to a 45° VHF and (b) features an 11.7° PD element coupled to a 22.5° VHF, when compared to the diffracted spectral curve of the VHF element alone (green). Furthermore, the simulated spectral diffraction curves closely match the actual spectral diffraction curves minus some slight structure. We can see that the diffraction curves are slightly red/blue shifted as apparent from measurements presented in System II, (b). This may be due to a slight misalignment in the PD element resulting in a shift of peak diffraction by ~10nm in the AVHF diffraction curve.

Optics EXPRESS

Demonstrated in Fig. (8) are images of the diffracted spectra from elements within AVHF System II. Fig. (8(a)) demonstrates mode m = 1 polychromatic diffraction across a predispersive element recorded at 11.7°. Figure (8(b)) demonstrates mode m = 1 polychromatic diffraction across a VHF element alone, recorded at 22.5°. Fig. (8(c)) demonstrates mode m = 1 polychromatic diffraction across a the AVHF system, where a PD recorded at the optimal angle, 11.7°, is coupled to a 22.5° VHF element. A clear distinction can be drawn between the diffraction spectra of the VHF element alone and the AVHF system. Clearly, through Fig. (7–8) we see the advantages of coupling the VHF to a optimized PD element.

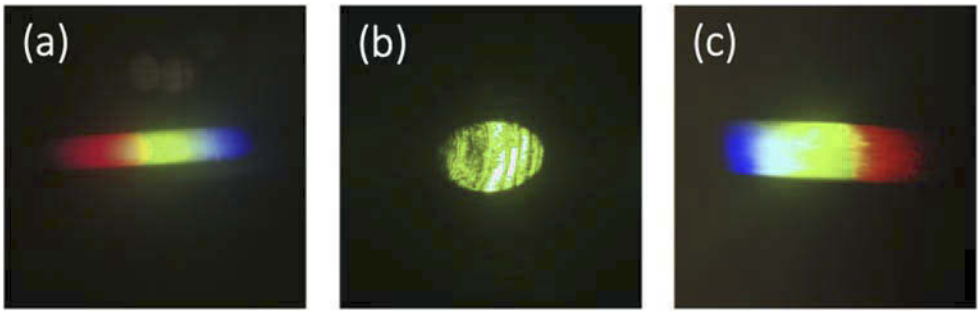

Fig. 8. Images demonstrating m = 1 polychromatic Bragg diffraction through (a) 11.7° PD element, (b) 22.5° VHF element alone, and a (c) 22.5° VHF in the AVHF configuration.

Presented in Table 2 are the diffracted spectral bandwidths of the AVHF systems compared to a VHF element alone. First, we can see that the empirical data closely match the simulated results. Furthermore, we can observe a substantial increase in spectral bandwidth with the optimized AVHF system where AVHF-SI has a 158x increase over a 45° VHF, with a spectral bandwidth of 32 nm. AVHF-SII has a 362x increase in spectral bandwidth with over a 22.5° VHF, with a spectral bandwidth of 108.6 nm. Previously we had reported spectral bandwidth of 35 and 70 nm for AVHF systems operating at 45° and 20°, with VHF elements with spectral selectivity of 9 nm and 8 nm. At this time, we have demonstrated an improvement by using i) very selective VHF elements (~25-40x more selective than previously demonstrated) whilst ii) managing to obtain AVHF spectral bandwidths 158-362x broader than the VHF elements alone (wherein previous works we manged to obtain 3.88-8.75x) [17].

Table 2. Denotes the recovered system spectral bandwidths for the the AVHF systems and the uncoupled volume hologram filters within those systems. E- is used to denote empirical data, S- is used to denote simulated data.

System	E-Spectral Bandwidth (FWHM)	S-Spectral Bandwidth (FWHM)
AVHF-SI	32 nm	33nm
45° VHF	0.202 nm	0.200 nm
AVHF-SII	108.6 nm	113.4 nm
22.5 ° VHF	0.300 nm	0.280 nm

The focus of the present work is the expansion of the spectral bandwidth of very thick spatio-spectral selective holograms. Here we did not asses or compensate spectral dispersion induced by the use of a holographic element (HOE); however, to compensate for the spectral dispersion of an HOE, another hologram can be used as it has been demonstrated by Jannson et. al. [26].

Optics EXPRESS

5. Conclusion

In this manuscript we have introduced the theoretical basis for predisperser to volume holographic filter coupling and have provided optimization of the AVHF diffracted spectral bandwidth. Furthermore, we provided experimental results that are in agreement with the simulated diffracted angular and spectral bandwidths of two AVHF systems operating at 45° and 22.5°. Being that the angular selectivity of the AVHF system is dependent on the VHF element, we expect to maintain, if not improve on, the depth-based wavefront selection capabilities of the AVHF system with a marked increase of 2-3 orders of magnitude for spectral diffraction bandwidth when compared to a VHF element alone.

Funding. U.S. Naval Research Laboratory, Remote Sensing Division, Radio, Infrared and Optical Sensors Branch, and Applied Technology Associates, Washington Operations.

Disclosures. The authors declare no conflicts of interest.

Data availability. Data underlying the results presented in this paper are not publicly available at this time but may be obtained from the authors upon reasonable request. Furthermore, see Supplement 1 for supporting content.

Supplemental document. See Supplement 1 for supporting content.

References

1. David Peri and Ritter Dan, "Spatial filtering with volume gratings," Appl. Opt. **24**(10), 1535–1540 (1985).
2. Yuan Luo, Paul J. Gelsinger, Jennifer K. Barton, Barbastathis George, and Raymond K. Kostuk, "Multiplexing Volume Holographic Gratings for a Spectral-spatial Imaging System," Proc. SPIE **6912**, 69120A8 (2008).
3. Li Zhenyu, Psaltis Demetri, Liu Wenhai, R. Johnson William, and Bearman Gregory, "Volume holographic spectral imaging," Proc. SPIE **5694**, 33–40 (2005).
4. Sunil Vyas, Chia Yu-Hsin, and Luo Yuan, "Volume holographic spatial-spectral imaging systems," J. Opt. Soc. Am. A **36**(2), A47 (2019).
5. Paul J Gelsinger-Austin, Luo Yuan, Jonathan M. Watson, Raymond K. Kostuk, Barbastathis George, Jennifer K. Barton, and Jose M. Castro, "Optical Design for a Spatial-spectral Volume Holographic Imaging System," Opt. Eng. **49**(4), 043001 (2010).
6. George Barbastathis, Balberg Michal, and J. Brady David, "Confocal microscopy with a volume holographic filter," Opt. Lett. **24**(12), 811–813 (1999).
7. Isela D Howlett, Han Wanglei, Gordon Michael, Rice Photini, Jennifer K Barton, and Raymond K. Kostuk, "Volume Holographic Imaging Endoscopic Design and Construction Techniques," J. Biomed. Opt. **22**(5), 056010 (2017).
8. Atsushi Sato, Scepanovic Miodrag, and Raymond K. Kostuk, "Holographic edge-illuminated polymer Bragg gratings for dense wavelength division optical filters at 1550 nm," Appl. Opt. **42**(5), 778–784 (2003).
9. Sunil Vyas, Wang Po-Hao, and Luo Yuan, "Spatial mode multiplexing using volume holographic gratings," Opt. Express **25**(20), 23726–23737 (2017).
10. Arnab Sinha and Barbastathis George, "Volume holographic telescope," Opt. Lett. **27**(19), 1690–1692 (2002).
11. Arnab Sinha, Sun Wenyang, Shih Tina, and Barbastathis George, "Volume Holographic Imaging in Transmission Geometry," Appl. Opt. **43**(7), 1533 (2004).
12. Arnab Sinha and Barbastathis George, "Broadband volume holographic imaging," Appl. Opt. **43**(27), 5214–5221 (2004).
13. Arnab Sinha, Barbastathis George, Liu Wenhai, and Psaltis Demetri, "Imaging Using Volume Holograms," Opt. Eng. **43**(9), 1959 (2004).
14. Zhi Chen, Gao Hanhong, and Barbastathis George, "Background suppression in long-distance imaging using volume hologram filters," Opt. Express **22**(25), 31123–31130 (2014).
15. A. Popov, I. Novikov, K. Lapushka, I. Zyuzin, Yu. Ponosov, Yu. Ashcheulov, and A Veniaminov, "Spectrally selective holographic optical elements based on a thick polymer medium with diffusional amplification," J. Opt. A: Pure Appl. Opt. **2**(5), 494–499 (2000).
16. Hanhong Gao, Jonathan M. Watson, Scott Stuart Joseph, and Barbastathis George, "Design of Volume Hologram Filters for Suppression of Daytime Sky Brightness in Artificial Satellite Detection," Opt. Express **21**(5), 6448 (2013).
17. Pedro Enrique Alcaraz and Blanche Pierre-Alexandre, "Advanced volume holographic filter to improve the SNR of polychromatic sources in a noisy environment," Opt. Express **29**(2), 1232–1243 (2021).
18. W. R. Klein and B. D. Cook, "Unified approach to ultrasonic light diffraction," IEEE Trans. Sonics Ultrason. **14**(3), 123–134 (1967).
19. S. Gallego, M Ortuño, C. Neipp, A. Márquez, A. Beléndez, I. Pascual, J.V Kelly, and J.T Sheridan, "Physical and Effective Optical Thickness of Holographic Diffraction Gratings Recorded in Photopolymers," Opt. Express **13**(6), 1939 (2005).

Optics EXPRESS

20. Jose M Castro, Brownlee John, Luo Yuan, Erich De Leon, Jennifer K. Barton, Barbastathis George, and K. K.ostuk Raymond, "Spatial-spectral Volume Holographic Systems: Resolution Dependence on Effective Thickness," Appl. Opt. **50**(7), 1038 (2011).
21. V. N. Borisov and A. V. Veniaminov, "Angular Selectivity of Amplitude-Phase Holographic Gratings in Polymer Material with Phenanthrenequinone," Opt. Spectrosc. **124**(6), 901–907 (2018).
22. L. Yuan, P. J. Gelsinger, J. K. Barton, G. Barbastathis, and R. K. Kostuk, "Optimization of Multiplexed Holographic Gratings in PQ-PMMA for Spectral-spatial Imaging Filters," Opt. Lett. **33**(6), 566–568 (2008).
23. H. Kogelnik, "Coupled Wave Theory for Thick Hologram Gratings," The Bell Syst. Tech. J. **48**(9), 2909–2947 (1969).
24. Y. Qi, E. Tolstik, H. Li, J. Guo, M. R. Gleeson, V. Matusevich, R. Kowarschik, and J. T. Sheridan, "Study of PQ/PMMA Photopolymer. Part 2: Experimental Results," J. Opt. Soc. Am. B **30**(12), 3308–3315 (2013).
25. V. N. Borisov and A. V. Veniaminov, "Determination of Refractive Index and Absorbance Modulation Amplitudes from Angular Selectivity of Holograms in Polymer Material with Phenanthrenequinone," Proc. SPIE **9545**, 954513 (2015).
26. Tomasz P Jannson, Tin M. Aye, and Gajendra D. Savant, "Dispersion and Aberration Compensation Techniques in Diffractive Optics and Holography," Proc. SPIE **2152**, 44–70 (1994).